RIA-76-U508

NSWC/WOL/TR 75-94

NSWC/WOL/TR 75-94

NSWC

TECHNICAL REPORT

WHITE OAK LABORATORY

INITIATION, DETONATION PROPAGATION, AND COMPUTATIONAL STUDIES FOR SUBMUNITIONS CONTAINING AMATEX-20

4 FEBRUARY 1976

NAVAL SURFACE WEAPONS CENTER
WHITE OAK LABORATORY
SILVER SPRING, MARYLAND 20910

- Approved for public release; distribution unlimited.

NAVAL SURFACE WEAPONS CENTER
WHITE OAK, SILVER SPRING, MARYLAND 20910

UNCLASSIFIED

SECURITY CLASSIFICATION OF THIS PAGE *(When Data Entered)*

REPORT DOCUMENTATION PAGE		READ INSTRUCTIONS BEFORE COMPLETING FORM
1. REPORT NUMBER NSWC/WOL/TR 75-94	2. GOVT ACCESSION NO.	3. RECIPIENT'S CATALOG NUMBER
4. TITLE *(and Subtitle)* Initiation, Detonation Propagation, and Computational Studies for Submunitions Containing Amatex-20		5. TYPE OF REPORT & PERIOD COVERED Final 6. PERFORMING ORG. REPORT NUMBER
7. AUTHOR(s) N. L. COLEBURN H. D. JONES H. M. STERNBERG		8. CONTRACT OR GRANT NUMBER(s)
9. PERFORMING ORGANIZATION NAME AND ADDRESS Naval Surface Weapons Center White Oak, Silver Spring, Maryland 20910		10. PROGRAM ELEMENT, PROJECT, TASK AREA & WORK UNIT NUMBERS NSWC-1267/AF
11. CONTROLLING OFFICE NAME AND ADDRESS		12. REPORT DATE 4 February 1976 13. NUMBER OF PAGES 35
14. MONITORING AGENCY NAME & ADDRESS *(if different from Controlling Office)*		15. SECURITY CLASS. *(of this report)* UNCLASSIFIED 15a. DECLASSIFICATION/DOWNGRADING SCHEDULE

16. DISTRIBUTION STATEMENT *(of this Report)*

Approved for public release; distribution unlimited

17. DISTRIBUTION STATEMENT *(of the abstract entered in Block 20, if different from Report)*

18. SUPPLEMENTARY NOTES

This research was monitored by the Air Force Armament Laboratory, AFATL/DLDE, Eglin AFB, Florida 32542

19. KEY WORDS *(Continue on reverse side if necessary and identify by block number)*

Explosives	Equation of State of High Explosives
Submunitions	Non-Ideal Explosives
Amatex	Explosion Hydrodynamics
Fragmentation	Detonations
Alternate Fills	

20. ABSTRACT *(Continue on reverse side if necessary and identify by block number)*

Computational and experimental support of Air Force alternate explosive fill development for the BLU-61 and BLU-63 submunitions is reported.

A scheme worked out for calculating the flow following detonation of Amatex-20 (20/40/40 RDX/TNT/AN) uses the JWL equation of state, together with an energy addition of 200 cal/g one (CONT)

DD FORM 1 JAN 73 1473 EDITION OF 1 NOV 65 IS OBSOLETE
S/N 0102-LF-014-6601

UNCLASSIFIED

SECURITY CLASSIFICATION OF THIS PAGE *(When Data Entered)*

microsecond after the detonation front has passed. Cylinder test data from several laboratories are compared and shown to be in good agreement. Casing breakup is estimated to occur after 46 % radial expansion in the BLU-61 bomblet and after 23% radial expansion in the BLU-63 bomblet. An aquarium experiment, detonation wave arrival measurements, and detonation parameter measurements are described. Amatex-20 with either 500 micron or 10 micron particle size AN is shown to be initiated satisfactorily with a standard A5 booster. No differences in booster initiation were observed when detonator base charge weights of 40 and 80 mg of PETN were used. Detonation velocity and detonation pressure measurements, made with small charges, are given.

The failure of Amatex-20 loaded bomblets to break up on some of the scored lines is attributed to the inferior metal fragmenting ability of this explosive, relative to the preferred fill.

NSWC/WOL/TR 75-94 4 February 1976

INITIATION, DETONATION PROPAGATION, AND COMPUTATIONAL STUDIES FOR SUBMUNITIONS CONTAINING AMATEX-20

This is a final report covering work extending over approximately a five month period, ending June 30, 1975, in support of an Air Force alternate explosive fills development program for the BLU-61B and the BLU-63B submunitions. The results are of more general interest, however, since they deal with computational and experimental aspects of research in non-ideal explosives.

The work was supported by the U.S. Air Force, under Task NSWC-1267/AF, Amatex-20 Detonation.

Julius W. Enig

JULIUS W. ENIG
By direction

TABLE OF CONTENTS

PART A

COMPUTATIONAL STUDIES

H. M. STERNBERG

PART B

EXPERIMENTAL STUDY OF AMATEX-20 INITIATION AND DETONATION

N. L. COLEBURN and H. D. JONES

ILLUSTRATIONS

TABLE OF CONTENTS
(Continued)

ILLUSTRATIONS
(Continued)

TABLES

PART A

COMPUTATIONAL STUDIES

H. M. STERNBERG

I. INTRODUCTION

Computational work with Amatex-20 (20/40/40 RDX/TNT/AN) was undertaken in connection with its potential use as an explosive fill for the BLU-61B and BLU-63B[1] bomblets. The general plan of the work was to use existing cylinder test data obtained at Picatinny Arsenal[2] (PA) and the Los Alamos Scientific Laboratory[3] (LASL) to get an equation of state scheme to use with Amatex-20 in explosion hydrodynamic calculations. Computations would then be made of the casing velocities of Amatex 20 loaded BLU-61B and BLU-63B bomblets.

The use of ammonium nitrate (AN) raises the possibility of a so called "non-ideal" detonation, i.e., part of the energy may be released after the detonation front has passed. In many applications this late energy release will not affect the conditions at the detonation front. It can be shown, however, that if the order of the reaction is equal to or greater than one, as is invariably the case, a steady state detonation is not possible[4], and the late energy release must ultimately affect the front if the charge diameter is considered to be infinite and the detonation is allowed to propagate indefinitely.

---

1. Bomb, Frag-BLU-61B, Dwg. No. 68D5900, and Bomb, Fragmentation BLU-63B or BLU-86B, Dwg. No. 68D5994, U. S. Air Force, Eglin AFB, Florida.
2. J. Hershkowitz and J. Rigdon, "Evaluation by a Modified Cylinder Test of Metal Acceleration by Non-Ideal Explosives containing Ammonium Nitrate" Picatinny Arsenal, Dover, New Jersey, Technical Report 4611, April 1974.
3. A. W. Campbell, R. P. Engelke, A. Popolato, and T. Rivera, "Physical and Processing Characteristics of Non-Ideal Explosives-Special Emphasis on Amatex (Task A), "Los Alamos Scientific Laboratory, Los Alamos, New Mexico, LA-57 11-PR Joint Services Explosives Program, Quarterly Report, March 16 through June 30, 1974, compiled by A. Popolato.

Definitions of the terms "at the detonation front" and "behind the detonation front" are needed to fix the ideas. At the detonation front will refer to points in the flow where the particle velocity plus the sound speed (u+c) is equal to or greater than the detonation velocity D. Behind the detonation front will imply $u+c<D$. It should be borne in mind that the distance between the point where $D=u+c$ and the detonation front will vary with the run distance (see Ref. 4).

For practical purposes it suffices to define "at the detonation front" and "behind the detonation front" more loosely, in terms of the measured detonation velocity and the measured velocities of shocks transmitted through normal impact on various inert materials in contact with the explosive (see, for example, Deal[5]). The transmitted velocities referred to are those that would be found in a specified test configuration, by extrapolating back to the explosive-inert material interface, with the effects of sharp reaction zone spikes ignored. Energy releases which influence one or more of these measurements will be presumed to have taken place at the detonation front. Energy releases which do not affect the detonation velocity or any of the transmitted shock velocities will be associated with flow behind the detonation front. In the same vein, it will be assumed that the Chapman-Jouguet (CJ) condition holds at the detonation pressure-particle velocity point determined by the transmitted shock experiments.

A number of models for the Amatex-20 detonation have been suggested. Mader[6] assumes that fifty percent of the AN reacts at the detonation front and that the remainder remains inert. Thermochemical calculations, assuming complete chemical equilibrium of the products from the elemental composition of the mixture of RDX, TNT, and reacting AN, then produce the observed detonation velocity and a reasonable detonation pressure. Kamlet[7] has proposed a model in which the AN and the RDX/TNT mixture both react completely but separately at the detonation front, each going to its own detonation products. One would then have a heterogeneous mixture of gas pockets in which further mechanical and chemical interaction takes place after the detonation front has passed. Hershkowitz and Rigdon[2] point out that the examination of wall expansion data from thin and thick walled cylinders shows that energy added to the system due to the AN must

4. H. M. Sternberg, "On the Mathematical Theory of the Chapman Jouguet State", Astronautica Acta, Vol. 15, pp 359-369, Pergamon Press, New York, 1970.
5. W. E. Deal, "Measurement of the Reflected Shock Hugoniot and Isentrope for Explosion Reaction Products", Phys. Fluids, Vol. I, No. 6, Nov-Dec 1958. Phys. Fluids 1, 523 (1958).
6. C. L. Mader, A. Popolato, and A. W. Campbell, "EOS of Amatex". Los Alamos Scientific Laboratory, Los Alamos, New Mexico, LA-5521-PR Joint Services Explosive Program, Quarterly Report, August 16 through November 30, 1973, compiled by A. Popolato.
7. Mortimer J. Kamlet. Private Communication.

appear before the cylinder walls have moved. For our purpose here this means that the additional energy must be added at the detonation front or very close behind it.

The computational model adopted here for use with Amatex-20 is based on the facts that its density, detonation velocity, and detonation pressure are close to those of TNT, but the wall velocities found in cylinder expansion work are somewhat greater than those obtained with TNT. To match these data an equation of state of the Jones-Wilkins-Lee (JWL) form[8], with constants chosen to give the correct detonation velocity and an estimated detonation pressure, was combined with an energy addition of 200 calories per gram to each computation cell one microsecond after the detonation front had passed through the cell. The short, one microsecond, delay might correspond to an induction time. This model, when used in the explosion dynamic computations to be described here gave results in good agreement with the existing experimental data. However, no claim is made for uniqueness. Other combinations of equations of state, equation of state constants, delay times, and energy releases, will no doubt work as well.

In Section II, the JWL equation of state constants for Amatex-20 are worked out, and the energy addition scheme used in the explosion dynamic calculations is described. Section III contains the existing cylinder expansion data, the calculated cylinder wall velocities, and a discussion of the relatively rapid acceleration of the cylinder wall observed at late times in the LASL work[3] with Amatex-20. The two-space dimension, transient, explosion dynamic computations to get the cylinder wall velocities were made with a computer code which is described in detail in a previous report[9]. This is a Lagrangian code that treats the cylinder wall as a collection of mass points, i.e., the metal mass is accounted for by increasing the masses associated with the outermost grid points. Otherwise the logic is similar in many respects to that of the HEMP code[10].

The results of the transient spherical flow calculations for the BLU61B and BLU63B bomblets are in Section IV.

II. EQUATION OF STATE SCHEME FOR AMATEX 20

For use in the explosion dynamics computations we need an equation of state of Amatex-20, together with mechanisms for creating the

---

8. Brigitta M. Dobratz, Ed., Properties of Chemical Explosives and Explosive Simulants, Lawrence Livermore Laboratory, University of California/Livermore, UCRL-51319, 15 December 1972.
9. H. M. Sternberg, "Computation of Weight, Velocity, and Angular Distributions of Fragments from Naturally Fragmenting Weapons" Naval Ordnance Laboratory, White Oak, Silver Spring, Maryland, NOLTR 74-77, 17 July 1974.
10. Mark L. Wilkins, "Calculation of Elastic-Plastic Flow," in methods of Computational Physics, Vol. 3, edited by B. Alder, S. Fernbach, and M. Rotenberg, Academic Press, New York, 1964.

detonation wave and for releasing additional energy due to chemical reaction behind the front.

The JWL form[8] was used for the equation of state. This can be written

$$p = A\left(1 - \frac{\omega}{R_1 V}\right)e^{-R_1 V} + B\left(1 - \frac{\omega}{R_2 V}\right)e^{-R_2 V} + \frac{\omega E}{V} \quad , \tag{1}$$

where p is the pressure, E is the internal energy per original cc, V is the relative specific volume ($= v/v_o$), and A,B,ω,R_1, and R_2, are constants. The corresponding expansion adiabat, with C constant, is

$$p = Ae^{-R_1 V} + Be^{-R_2 V} + CV^{-(\omega + 1)} \tag{2}$$

The constants A, B, and C give p in megabars.

Reference 8 contains a table of constants for various explosives, for use in the JWL equation. For most common military explosives containing only carbon, hydrogen, oxygen, and nitrogen, (CHNO) R_2 is between 0.9 and 1.2, ω is about 0.35, and R_1 is between 4.2 and 4.6. A choice of R_1 outside of a small range, which is different for different explosives, will cause the condition that the sound speed be positive to be violated as the gas expands. In general, increasing the value of R_1 inside this permissible range, with a corresponding change in A and B to keep the detonation conditions fixed, will have practically no effect on the expansion from the CJ state to V=1. The larger value of R_1 will, however, cause the gas to do more work in the expansion from about V=1 to V=5, and less for $V > 5$.

The procedure adopted here has been to fix R_1, R_2, and ω, and to use the detonation velocity, the detonation pressure, and the energy released at the detonation front to get A, B, and C in Eq. (2). This was done as follows:

Consider a layer of gaseous detonation products at the detonation front and its behavior when the time is too short for later energy additions to have an influence, e.g., when a shock is transmitted into a low density material. Assume that the extremely rapid expansion that occurs here is isentropic and that it starts at the CJ state. One then has, neglecting the ambient pressure ahead of the detonation front,

$$p_J = \rho_o D u_J \tag{3}$$

$$D = u_J + c_J \tag{4}$$

$$V_J D = D - u_J = c_J \tag{5}$$

$$(dp/dV)_J = -\rho_o c_J^2/V_J^2 = -\rho_o D^2 \tag{6}$$

$$E_J = Q + p_J (1 - V_J)/2 \tag{7}$$

Here u is the particle velocity, c is the sound speed, ρ_o is the density of the undetonated explosive, and the subscript J denotes the CJ condition. In Eq. (7), Q is the energy released by the explosive at the detonation front (mbar-cc/original cc). It does not include any later energy addition.

The energy E_J in Eq. (6) being the work done in the complete expansion of the gas from the CJ state is

$$E = \int_{V_J}^{\infty} p \, dV \tag{8}$$

Equation (2), together with its derivative and integral, and Eqs. (3)-(8), now lead to three linear equations which can be solved for A, B, and C, once ρ_o, D, p_J and Q are specified (recall that R_1, R_2, and ω are chosen in advance). These equations are:

$$e^{-R_1 V_J} A + e^{-R_2 V_J} B + V^{-(\omega + 1)} C = p_J \tag{9}$$

$$R_1 e^{-R_1 V_J} A + R_2 e^{-R_2 V_J} B + (\omega + 1) V_J^{-(\omega + 2)} C = \rho_o D^2, \tag{10}$$

$$\frac{e^{-R_1 V_J}}{R_1} A + \frac{e^{-R_2 V_J}}{R_2} B + \frac{V_J^{-\omega}}{\omega} C = Q + p_J / (2 \rho_o D) \tag{11}$$

The density ρ_o = 1.603 g/cc and the detonation velocity D = 0.7030 cm/μsec were used for Amatex 20 (see Refs. 2 and 3) in Eqs. (10) and (11). The detonation pressure needed in Eqs. (9) and (11) was estimated with the Kamlet formula[11] for CHNO explosives, viz.,

11. Mortimer J. Kamlet and S.J. Jacobs, "Chemistry of Detonations, I. A Simple Method for Calculating Detonation Properties of C-H-N-O Explosives," J. Chem. Phys. vol. 48, pp 23-35, 1968.

$$p_J = 1.53\ [D/(1.30 + 1/\rho_o)]^2 \qquad (12)$$

with D in cm/μsec, ρ_o in g/cc, and p_J in mbar.

With the D and ρ_o values given above the value $p_J = 0.204$ megabars was calculated from Eq. (12). The constants R_1, R_2, and ω were taken as 4.6, 1.0, and 0.35 respectively. The energy release at the detonation front was arbitrarily set at Q = 0.0536 mbar-cc/original cc (800 calories per gram). The solution of Eqs. (9)- (11) was then

A = 4.9521 B = 0.08058 C = 0.001954.

The equation of state Eq. (1) was augmented with a simple scheme for bringing the effects of the chemical reactions into the explosion dynamic computations. Note below that all of the energy that will eventually be used is put into each computation cell originally, but only part of this energy may be used to calculate the pressure, depending upon the values of the progress variables F_1 and F_2, which are initially zero.

If Eq. (1) is written

$$p = f\ (E, V) \qquad (13)$$

then the form used in the computations is

$$p = f\ (\tilde{E}, V)\ F_{1K} \qquad (14)$$

where F_{1K} is a burn fraction corresponding to the fraction of the computation cell considered detonated (see the description of the HEMP code[10]), and

$$\tilde{E} = E - (1 - F_{2K})\ Q_2 . \qquad (15)$$

The variable F_{1K} is calculated from

$$\begin{cases} \tilde{F}_1 = \max \left\{ (D \cdot T - Z_{K,o})/(Z_{K+1,o} - Z_{K,o}),\ (1 - V_{K,o})/(1 - V_J), \right\} \\ F_1 = \min \left\{ 1,\ \tilde{F}_{1K}/r \right\} . \end{cases} \qquad (16)$$

where Z is the axial distance, k is the Lagrangian label for the grid points in the axial direction, and T is the time from the start of the detonation at Z = 0. The value 1.0 was used for r.

The constant Q_2, in Eq. (15), is the additional energy per original cc, added behind the detonation front. The progress variable F_2 would, in more complicated cases, be found by integrating the reaction rate dF_2/dt, which would be a function of the equation of state variables. In the present calculations F_2 remains equal to zero until a specified number of microseconds after the detonation front has passed the k'th cell. At this time, all of the additional energy Q_2 is made available for the pressure calculation by abruptly changing F_2 from zero to one.

Note above that the total energy put into each cell at the outset is $Q + Q_2$. However, this is not all available for the pressure calculation until both F_1 and F_2 become equal to one.

In the hydrodynamic computations, Eqns. (14) and (15) are used together with

$$dE + (p + q)\, dV = 0$$

to find p and E, once V is known. The variable q is the artificial viscosity.

Table I is a summary of the JWL form equation of state and the related computational scheme worked out for Amatex-20. The additional energy Q_2 was taken equal to 200 calories per gram because this resulted in calculated cylinder wall velocities which matched the existing data (see Section III).

TABLE I

Equation of State Scheme Used for Amatex-20

JWL Equation of State

$$p = A\left(1 - \frac{\omega}{R_1 V}\right) e^{-R_1 V} + B\left(1 - \frac{\omega}{R_2 V}\right) e^{-R_2 V} + \frac{\omega E}{V},$$

$\omega = 0.35$ $\quad A = 4.9521$

$R_1 = 4.6$ $\quad B = 0.08058$

$R_2 = 1.0$

$\rho_o = 1.603$ g/cc, $D = 0.7030$ cm/μsec, $V_J = 0.7425$

$E_o = Q + Q_2 = 0.0675$ mbar-cc/original cc (1000 cal/g)

$Q = 0.0536$ mbar-cc/original cc (800 cal/g)

$Q_2 = 0.0139$ mbar-cc/original cc (200 cal/g)

For detonation wave computation

$$p = f\,(\tilde{E},\ V)\ F_{1K}$$

$$\tilde{E} = E - (1 - F_{2K})\ Q_2$$

$$\tilde{F}_{1K} = \max\left\{(D\cdot T - Z_{K,o})/(Z_{K+1,o} - Z_{K,o}),\ (1 - V_{K,o})/(1 - V_J)\right\}$$

$$F_{1K} = \min\left\{1,\ \tilde{F}_{1K}/r\right\},\ r = 1.0$$

$$F_{2K} = \begin{cases} 0, & T < T_K + 1\ \mu\text{sec} \\ 1, & T \geq T_K = 1\ \mu\text{sec} \end{cases}$$

T_K = time detonation front reaches the end of the k'th computation cell.

III. CYLINDER TESTS

A great deal of testing has been done with a Lawrence Livermore Laboratory (LLL) configuration described in the Fourth Detonation Symposium volume[12]. This consists of a one inch inside diameter copper tube, 12 inches long, with a 0.1022 inch wall thickness. The explosive is plane detonated at one end and the position of the outside wall versus time in a plane perpendicular to the axis and seven inches from this end is found from streak camera records. This is differentiated to get the outside wall velocity in the observation plane.

The LLL cylinder test, scaled up to a four inch inside diameter, was used at both PA[2] and LASL[3] to determine the metal accelerating abilities of Amatex-20 and Amatex-40 (40/40/20 RDX/TNT/AN) relative to a standard. The velocity data from the Amatex-20 loaded cylinders, with explosive/metal mass close to 0.4, will be used here to get the energy to be added behind the detonation front in the explosion dynamic computations. Before doing this the data from the different laboratories will be compared.

The variations in the compositions of the standards used at the different laboratories are insignificant. The standard used at PA was 60/40 Cyclotol (60/40 RDX/TNT). The 60/40 refers to the starting percentages, by weight, in the formulation process. The finished explosive is in the 61/39 to 64/36 range. The standard used at LASL and LLL was Composition B, Grade A. Here the starting materials are 59.5/39.5/1.0 RDX/TNT/Wax. At LASL, the finished explosive is about 63/37/0.4 RDX/TNT/Wax[13]. In the LLL table of equation of state constants[8] 64/36 RDX/TNT is listed for Composition B, Grade A. The measured solid explosive densities were 1.694 g/cc in the PA work[2], 1.701 at LASL[3], and 1.717 at LLL[12].

Figure 1 contains plots of the outer wall velocities reported by the three laboratories for the 60/40 Cyclotol and Composition B, Grade A, all scaled to the four inch inside diameter cylinder. Both the PA and the LASL measurements were made in a plane 24 inches from the booster end of the cylinder. The corresponding scaled distance for the LLL work is 28 inches. Calculations show that $R-R_o$ versus t at the two positions should be essentially the same. Only two of the LLL velocities are shown in Fig. 1. These are the velocities listed in Ref. 12. Note in Fig. 1, that at $R-R_o$ = 76 mm (the 19 mm in the LLL test scaled to a four inch I.D. cylinder), the LLL and LASL velocities are practically identical, and the PA velocity is about one percent greater. At $R-R_o$ = 104 mm the PA velocity is about two percent greater than the LASL velocity.

12. J.W. Kury, H.C. Hornig, E.L. Lee, J.L. McDonnel, D.L. Ornellas, M. Finger, F.M. Strange, and M.L. Wilkins, "Metal Acceleration of Chemical Explosives," in Proc. Fourth Symp. (International) on Detonation, Office of Naval Research, Rpt. ACR-126, U.S. Gov't Printing Office, Washington, D.C. 1965.
13. A. Popolato. Private communication.

Outer cylinder wall velocities obtained by PA[2] and LASL[3] with Amatex-20, in the LLL test scaled to the four inch I.D., are also shown in Fig. 1. At $R-R_o$ = 76 mm, the LASL velocity is about three percent lower. However, between $R-R_o$ = 90 mm and $R-R_o$ = 115 mm the LASL data contains a rapid increase in velocity which does not appear in the PA work.

In connection with the possibility of very late energy addition due to chemical reaction, it is of interest to estimate how much energy would have to be added to the system in order to produce the rapid velocity increase observed in the LASL work.

To make this estimate, assume radial flow with uniform pressure p, density ρ, and internal energy E, which are functions of time only. Treat the metal as a tube with the correct mass, but no thickness. Assume also that the gas obeys a γ law, and expands adiabatically, in the time interval $t_1 \leq t \leq t_2$, where the subscripts 1 and 2 mark the ends of the rapid acceleration period. Let R be the radius of the metal cylinder and u the velocity (= $d\tilde{R}/dt$). The equation of motion can then be written

$$\frac{\tilde{R}_o \rho_o}{2C/M} \frac{du}{dt} = \tilde{R}p, \tag{17}$$

where ρ_o is the solid explosive density, C/M is the solid explosive mass/metal mass, and $\tilde{R}$ is the initial radius. The gas behavior assumptions imply

$$p/p_1 = (\rho/\rho_1)^{\gamma} \tag{18}$$

and the conservation of mass requires

$$\rho/\rho_1 = \tilde{R}_1^2 / \tilde{R}^2. \tag{19}$$

From (17) - (19),

$$K \, dZ/Dt = p_1 \, r^{1-2\gamma}, \tag{20}$$

where $K = \tilde{R}_o \rho_o / (2C/M)$, $r = \tilde{R}/\tilde{R}_1$ and $Z = dr/dt$.

Equation (20) has the integral

$$\frac{K}{\tilde{R}_1^2}\left[u_2^2 - u_1^2\right] = \frac{p_1}{\gamma-1}\left[1 - r_2^{2(1-\gamma)}\right]. \tag{21}$$

Suppose that additional internal energy is added abruptly at time t_1. This will increase the pressure but leave the velocity and density at $t=t_1$ unchanged. Call the quantities changed by the energy addition E_1, p_1, u_2, r_2. The γ law assumption means

$$E_1 = \frac{p_1}{\rho_1(\gamma-1)} \quad \text{and} \quad \hat{E}_1 = \frac{\hat{p}_1}{\rho_1(\gamma-1)}. \tag{22}$$

From Equation (21),

$$\frac{K}{\tilde{R}_1^2}\left[\hat{u}_2^2 - u_1^2\right] = \frac{\hat{p}_1}{\gamma-1}\left[1 - r_2^{2(1-\gamma)}\right]. \tag{23}$$

At the same radial expansion ($r_2=\hat{r}_2$), using (21)-(23),

$$\frac{\hat{E}_1}{E_1} = \frac{\hat{u}_2^2 - u_1^2}{u_2^2 - u_1^2}. \tag{24}$$

In Fig. 1 the LASL wall velocity of the Amatex-20 loaded cylinder is 1.485 mm/μsec (this is u_1) at $R-R_o=90$ mm. The velocity u_2 at $R-R_o=115.6$ mm is 1.560 mm/μsec. The extrapolated velocity at $R-R_o=115.6$ mm, taken from the dashed section in Fig. 1, is 1.510 mm/μsec. This is u_2. With the above values for u_1, u_2, and $\hat{u}_2$, we get, with Eq. (24),

$$\hat{E}_1/E_1 = 3.05. \tag{25}$$

Transient explosion dynamic computations in two-space dimensions show that at $R-R_o=90$ mm about 15% of the chemical energy released in the early stages remains as internal energy of the gas. Using this value, together with the energy release in Table I (1000 cal/g) and Eq. (25), shows that about 300 additional calories per gram would have to be added at $R-R_o=90$ mm in order to produce the velocity increase observed in the $R-R_o=90$ to 115 mm range.

The computer program, MASSPT described in Ref. (9) was used for the explosion dynamic computations involving the cylinder test configuration. This program treats the metal as a tube with mass

but no thickness, i.e., as a set of grid points with extra mass, whose motions are found along with the gas flow. The gas dynamics following detonation is Lagrangian, with provision for slippage along the metal boundary. Additional routines, not needed in the weapon calculations described in Ref. (9), were added in order to permit the gas to flow out of the ends of the cylinder. In the computation the cylinders were 4 inches in inside diameter, 38 inches long (36 inches plus 2 inches for the plane wave initiator), and plane initiated at one end. A 100X6 computation grid was used, making the computation cells 0.847 cm in the radial direction and 0.965 cm in the axial direction. To compensate for the coarse zoning the energy was released more quickly than in the HEMP code[10], by taking r in Eq. (16) equal to 1.0, instead of the 2.5 value suggested in Ref. (10).

The MASSPT code gives the motion of a mass tube of zero thickness. The motion of the outside wall must be gotten from this for comparison with the experimental data. Let R be the outside radius, $\tilde{R}$ the inside radius, and use the zero subscript for the initial conditions. Assume the metal is incompressible. Then the outside and inside wall radii and velocities are related by

$$R^2 - \tilde{R}^2 = R_o^2 - \tilde{R}_o^2 \ , \tag{26}$$

and, using Eq. (26),

$$\frac{dR}{dt} = \frac{\tilde{R}}{R} \frac{d\tilde{R}}{dt}. \tag{27}$$

Also, if r is a variable radius between the inner and out walls,

$$R^2 - r^2 = R_o^2 - R_o^2 \quad \text{and} \quad \frac{dR}{dt} = \frac{r}{R} \frac{dr}{dt}. \tag{28}$$

The outer wall velocity in the observation plane was found here from the calculated mass point velocity by assuming that the kinetic energy of a section of the tube is equal to the kinetic energy of the corresponding mass point, counting only the radial velocity. We then have, with v the calculated radial velocity of the mass point, and the metal assumed incompressible,

$$2 \int_{\tilde{R}}^{R} \left(\frac{dr}{dt}\right)^2 r \, dr = (R^2 - \tilde{R}^2) v^2 \ . \tag{29}$$

Equations (28) and (29) lead to the outer wall velocity

$$\frac{dR}{dt} = \left[\frac{1 - (\tilde{R}/R)^2}{2\ \ell n(R/\tilde{R})}\right]^{1/2} \nu \ , \tag{30}$$

where $\tilde{R}$ is the radial position of the mass point and R and $\tilde{R}$ are related by Eq. (26). A very close approximation to Eq. (30), in the range of interest, is

$$\frac{dR}{dt} = \frac{1}{2}\left[1 + \frac{\tilde{R}}{R}\right] \nu. \tag{31}$$

The curves in Fig. 1 are plots of velocity versus distance calculated with the MASSPT program for the plane perpendicular to the axis of the copper cylinder and 26 inches from the initiation end. Twenty six inches, instead of 24, were used here in order to take the plane wave booster into account. The calculated mass point velocities were corrected with Eq. (30) to get the plotted outer wall velocities. The use of this correction, which implies a uniform metal density and instantaneous communication between the inner and outer cylinder walls, probably accounts for the calculated outer wall velocities being a bit higher than the experimental values during the early motion.

The calculations for the cylinders containing TNT and 60/40 Cyclotol were made with the JWL equation of state and the JWL equation of state constants listed in Ref. (8). The Composition B, Grade A constants in Ref. (8) and the solid explosive density ρ=1.701 g/cc was used to model both the PA and LASL experiments. This density is the experimental value reported for the LASL charges[3].

The calculated results shown for Amatex-20 in Fig. 1 were obtained with the equation of state scheme in Table I. This has the JWL form with the constants found by the method in Sec. II. Also (see Table I), in order to match the experimental data, 200 cal/g were added to each computation cell one microsecond after the detonation front passed through it. This choice produces velocities at $R-R_o$=76 mm that are roughly midway between the LASL and the PA values.

If one wanted a computation scheme that would produce only the LASL results for Amatex 20 in the 4 inch I.D. cylinder including the very late acceleration (Fig. 1), then an extension of Eq. (15) could be used, namely,

$$\tilde{E} = E - (1 - F_2)\ Q_2 - (1 - F_3)\ Q_3 .$$

Here, Q_2= 150 cal/g, Q_3=300 cal/g, F_2 and F_3 are zero initially, F_2 is set equal to one after a one microsecond delay, and F_3 is set equal to one when $R-R_o$=90 mm in the cross section intersecting the computation cell. The total energy release, including the 800 cal/g at the detonation front, would then be 1250 cal/g. This is reasonable for the elemental composition of the solid explosive. However, a rationale for the very late energy release is missing.

IV COMPUTATIONS FOR BOMBLETS

The BLU-61B and BLU-63B bomblets are small spherical steel shells (consisting of two hemispherical shells fastened together) containing a grenade fuze, a booster and a high explosive fill. The fragment size is determined by scoring the metal surface. The fuze initiates the booster at an off axis spot about one half inch from the center.

Transient, one space dimension, spherical flow calculations were made with a Lagrangian, artificial viscosity, explosion dynamics code. Fifty computation cells were used. The innermost grid point was fixed at 1.27 cm from the center for the entire computation, i.e., the fuze was modeled by a rigid sphere with a one half inch radius, and a spherical detonation wave was initiated on the surface of this sphere. The artificial viscosity was a sum of a linear and a quadratic function of the particle velocity. The metal casing was modeled by adding its mass to the mass associated with the outermost grid point. Dimensions used in the computations for the BLU-61B and the BLU-63B munitions are shown in Fig. 2. The equations of state used for the cylinder expansion calculations described in Sec. III, were used here namely, the scheme for Amatex-20 listed in Table I, and the JWL equation for Composition B, Grade A listed in Ref. (8) (with ρ_o=1.701g/cc and the corresponding E_o=0.0842 mbar-cc/orig. cc).

The hemispheres of the submunitions move apart initially before they break up. This results in some venting of the product gas and a rarefaction wave which moves inward and effects the metal velocity near the edges of the hemispheres. This rarefaction and the related pressure drop are ignored in the transient one space dimension calculations.

Figures 3 and 4 contain plots of the calculated casing velocity versus inside radius. Note that the velocity keeps increasing because there is nothing in the computation to account for the fragmentation of the casing. To get a calculated fragment velocity, one must decide, usually from photographic evidence, upon the radius at which the casing breaks up into fragments and acceleration essentially stops. This radius is not available here. We can, however, try to work back from the observed fragment velocities in order to estimate the radius where the casing breaks up.

The initiation spot, in the grenade fuze, is approximately one half inch from the center and 70 degrees from the pole of one of the hemispheres. Fragment velocities were estimated by Ramsay[14] at LASL, from flash radiographs. For Amatex 20 loaded bomblets the estimated velocities at the 70 degree position were 1.37±0.05 mm/μsec (4495±164 ft/sec) for the BLU-61B munition and 1.1±0.05 mm/μsec (3609±164 ft/sec)for the BLU-63B munition. Figs. 3 and 4 show that these velocities correspond to acceleration cessation, due to casing break up, at 46% radial expansion (5.2 cm inner radius) for the BLU-61B munition and at 23% radial expansion (3.2 cm inner radius) for the BLU-63B munition. The 0.05 mm/μsec standard deviation in the measured velocity corresponds to a 3-4% change in the radial expansion when the casing breaks up.

In the cylinder test experiments[2,3] it was shown that the substitution of 40 parts of AN for RDX in 60/40 Cyclotol, to make Amatex-20, resulted in a kinetic energy imparted to the metal ratio of 0.83-0.85. This ratio can be estimated for the munitions considered here, from Figs. 3 and 4, by assuming that the kinetic energy ratio is the square of the calculated velocity ratio. This leads to kinetic energy ratios of 0.86-0.88 for the BLU-61B munition and 0.81-0.87 for the BLU-63B munition. The exact values, in these ranges, depend upon the radial expansion when acceleration ceases. If the dashed vertical lines in Figs. 3 and 4 are used (46% radial expansion for the BLU-61B and 23% for the BLU-63B), the calculated ratios are 0.88 for the BLU-61B and 0.81 for the BLU-63B munitions.

V REMARK ON FRAGMENTATION

Amatex-20 has been found unsuitable for use in the BLU-61B and the BLU-63B munitions because the casings do not break along some of the scored lines and significantly more multiple fragments result than are obtained with the preferred fill (60/40 Cyclotol). At one time it was thought that this could be explained in terms of the small size of the systems and the run distance needed to get the detonation fully started. This does not appear to be the case (see Part B of this report).

A plausible explanation for the greater number of multiple fragments found when Amatex-20 is used lies in the fact that the ability of this explosive to fragment metal is inferior to that of the 60/40 Cyclotol. The density, detonation velocity, and detonation pressure of Amatex-20, which affect the fragmentation are very much like those of TNT. The values of these quantities that we have been using here for Amatex-20, TNT, and 60/40 Cyclotol (see Sec. II and Ref. 8) are listed in Table II.

---

14. J.B. Ramsay, Bomb Performance Tests, in "Feasibility of Using Amatex in Small Bombs, Progress Report Sep 1 through Oct 31, 1974, AFATL project order 4-065Q-11" University of California, Los Alamos Scientific Laboratory, WX-3, Dec 6, 1974, letter report compiled by A. Popolato.

Table II

Densities, Detonation Velocities, and Detonation Pressures of Amatex 20, TNT, and 60/40 Cyclotol

	Amatex 20	TNT	60/40 Cyclotol
ρ_o (g/cc)	1.603	1.630	1.701
D (cm/μsec)	0.703	0.693	0.798
p (mbar)	0.204	0.210	0.295

Reference (15) lists the relative fragmentation abilities of various explosives in terms of the average weight of fragments $\bar{M}$, weighing more than one grain, recovered in a particular test configuration. Values of $\bar{M}$ obtained there are 17 grains for cast TNT and 12 grains for Composition B, which, except for a fraction of one percent of wax, is identical to 60/40 Cyclotol. From Table II we can expect that the Amatex-20 will have about the same ability to fragment metal as TNT. We can therefore assign values of $\bar{M}$ equal to 17 grains for Amatex-20 and 12 grains for the preferred fill (60/40 RDX/TNT). This indicates that the metal fragmenting ability of the preferred fill is substantially better than that of the Amatex-20. It is most likely the reason for the greater number of multiple fragments observed with Amatex-20 than with 60/40 Cyclotol.

VI CONCLUSIONS

An equation of state scheme for Amatex-20 which combines a JWL equation with an energy addition of 200 cal/g one microsecond after the detonation front has passed can be used in hydrodynamic calculations with satisfactory results.

Cylinder test wall velocities from LASL, PA, and LLL agree within 2 percent for 60/40 Cyclotol, for expansions to twice the initial diameter. For Amatex-20 in four inch I.D. cylinders the measured PA wall velocity is about 3 percent greater than the LASL velocity at $R-R_o$ = 76 mm.

A rough estimate shows that an abrupt addition of about 300 cal/g to the detonation products of Amatex-20 is needed to produce a wall velocity increase observed between $R-R_o$ = 90 mm and $R-R_o$ = 115 mm in the LASL four inch I.D. cylinder tests.

15. H.M. Sternberg, "Fragment Weight Distributions from Naturally Fragmenting Cylinders Loaded with Various Explosives" Naval Ordnance Laboratory, White Oak. Silver Spring, Maryland 20910, NOLTR 73-83, 12 October 1973.

Results of hydrodynamic computations combined with bomblet fragment velocities measured at LASL from flash radiographs indicate that casing rupture to form fragments occurs after 46 percent radial expansion in the BLU-61B and after 23 percent radial expansion in the BLU-63B bomblets.

The failure of Amatex-20 loaded bomblets to break on some of the scored lines is probably due to the inferior metal fragmenting ability of this explosive, relative to the preferred fill.

PART B

EXPERIMENTAL STUDY OF AMATEX-20 INITIATION AND DETONATION

N. L. COLEBURN and H. D. JONES

I. INTRODUCTION

Measurements of the initiation and detonation of Amatex-20 (20/40/40 RDX, TNT, AN), using standard boostering systems, were made to give some insight into the fragmentation results obtained when this explosive is used as a fill in the BLU-61B and the BLU-63B munitions (bomblets). In fragmentation tests the munition casings failed to break along some of the scored lines, with resulting multiple fragments. It was felt that this might be connected with the response of the explosive to the type and strength of the boostering, detonation propagation from asymmetrical initiation, or AN particle size effects. The relative insensitivity and lower energy output of Amatex-20,compared with the preferred fill, were also possible causes for the inadequate fragmentation performance.

II. EFFECT OF DETONATOR BASE CHARGE WEIGHT ON THE INITIATION OF AMATEX-20 BY STANDARD BOOSTERS

In the first phase of the initiation study, the aquarium technique and high speed streak camera photography were used to study the effect of variations in the strength of the shock from a detonator. Mark 70 detonators, containing a base charge of 80 mg of PETN, and Mk 71 detonators, containing a base charge of 40 mg of PETN, were used. The tests consisted of measuring the lateral and axial shock output from A-5 boosters in an experimental setup similar to the boostering arrangement in the bomblets. The boosters were cylindrical pellets with an L/D of 0.3. Two pellet sizes were used, 15.3 mm in diameter by 5.2 mm long, and 13.0 mm in diameter by 4.2 mm long. The average densities were 1.70 g/cc and 1.62 g/cc, respectively.

The charge arrangement is shown in Figure 5A. The detonator was inserted into an aluminum holder and was held in contact with one face of the boostering pellet. The detonator was offset from the center of the booster face so that intiation occurred first at a point 3.1 mm from one edge. The arrangement was positioned in a Plexiglas-walled aquarium and aligned with the smear camera slit at 90 degrees with respect to the booster side and at the midpoint of the booster.

Figure 5B is a typical record from the experiment where a 12.7 mm diameter A-5 booster was used. The camera writing speed was ∿4mm/μsec. The first event seen in Figure 5B is the detonation wave arrival on the side of the booster as viewed through the camera slit. The record shows, as expected, earliest time arrival for the wave emerging from the booster edge which was closest to the point of initiation. The maximum arrival time difference between detonation breakout on the sides of the cylindrical booster was ∿0.4 microsec. The lateral shock traces in the water also are clearly delineated in Figure 5B. Note the large differences in the initial decay of the shock wave propagation from each side of the booster.

Shock-wave velocities were obtained by differentiating the distance-time data derived from microcomparator readings of the shock traces in Figure 5B. The velocities were converted to peak pressures from knowledge of the shock Hugoniot for water[16]. Figures 6 and 7 show the lateral peak pressure outputs and shock wave decay derived from the measurements. The curves in Figure 6 were obtained from measurements of the weaker lateral shock (upper trace in Figure 5B) which propagates from the side of the cylindrical booster closest to the point of initiation. Similarly the "strong shock" curves of Figure 7 are the results of measurements of the shock wave which originated when the detonation wave reached the side farthest from the point of initiation. The peak pressure results plotted in Figure 2 show little difference in output from the Mk 70 and Mk 71 detonators. In the "strong shock" graph, Figure 7, an anomaly results. The lateral output from the Mk 71 detonator is greater than the output from the Mk 70 detonator which contains the larger base charge weight of PETN. This result may be due to the experimental error in the measurements and the difference in the densities of the booster charges. The density of the charge fired with the Mk 71 detonator was 1.819 g/cm^3 while the booster initiated by the Mk 70 detonator had a density of 1.758 g/cm^3. The "strong" shock output results from the detonation propagating through a greater thickness of explosive and thereby would be more affected by the density difference than the "weak" lateral shock output.

III. DETONATION WAVE ARRIVAL MEASUREMENTS

The smear camera arrangement shown in Figure 8 was used to observe the detonation wave arrival in Amatex-20. Measurements were made of wave arrivals on the charge sides and on the charge face opposite the detonator. As shown in the figure, an A-5 booster was imbedded flush with one face of the cylindrical Amatex-20 charge. Charges containing 500 micron AN and charges containing 10 micron AN were fired. Fine scratch marks were cut ∿1 mm deep on the charge

(16) M. H. Rice and J. M. Walsh, J. Chem. Phys. 26, 824 (1957)
(17) N. L. Coleburn, "The Chapman-Jouguet of Several Pure and Mixed Explosives", NOLTR 64-58, 25 June 1964

surface at 1.27 cm intervals, and covered with scotch tape. Detonation wave arrival at these points produced the sharp pips noted in the smear camera trace of Figure 9.

The detonation wave arrival profiles on the faces of the charges were somewhat different for charges containing the two different ammonium nitrate particle sizes. The wave front from the 500 micron AN charges first arrived on the face at the center. The wave front from the 10 micron AN charges arrived on the face at the point offset about 3 mm from the center. In both cases, subsequent arrivals of the wave front were symmetric about a line perpendicular to the face through the point of first arrival (see Figure 10). Approximate detonation velocities determined from the breakout on the charge sides (see the top and bottom traces in Figure 9) are a few percent greater for the charges containing 10 micron AN. Also measurements of the smear camera traces in Figure 9 showed that the velocity of the circular wave front on the charge face is a bit greater for the 10 micron AN charge.

IV. DETONATION PARAMETER MEASUREMENTS

Measurements of the detonation velocity and detonation pressure of Amatex-20 were made using cylindrical charges containing AN with 500 micron particle size. The detonation velocity was measured directly and the detonation pressure was inferred from shock wave measurements using the aquarium technique described in reference (17). In these measurements all charges were eight inches long and two inches in diameter. Boostering was accomplished by a one-inch high, two-inch diameter pentolite-baratol plane wave booster. Wave curvature effects on the detonation measurements due to an inadequate L/D (length to diameter) were minimized by the above initiation. The charges were confined in 2.00-inch diameter copper cylinders with 0.233-inch thick walls. Holes of 0.1-inch diameter were drilled through the cylinder wall on a line extending down the cylinder length at 0.5-inch intervals. The holes were filled with pressed RDX and covered with scotch tape. By aligning the smear camera slit to bisect the holes and to extend beyond the end of the charge, the detonation velocity of the explosive and the velocity of the shock transmitted into the water from the end of the charge were measured. Cast charges with densities of 1.603 ± 0.002 g/cm^3 were used. The detonation velocity measured was 6790 ± 20 m/sec. The initial shock velocity in the water was 5440 ± 35 m/sec. The corresponding pressure, P_{H_2O} and particle velocity u_{H_2O} are 121 kbar and 2250 m/sec respectively. The detonation pressure P_J, is given by solving by iteration the equations

$$P_J = P_{H_2O}\left[1 - \frac{(k^2 - 1)u_{H_2O} - (k-1)D}{2kD}\right]^{-\frac{2k}{k-1}},$$

$$P_J = \frac{\rho_o D^2}{k+1},$$

where k is the isentropic exponent, D the detonation velocity and ρ_o, the charge density. Substituting the above values in these equations yields P_J = 179 kbar and k = 3.12 for cast Amatex-20 with 500 micron AN particle size. The densities of the charge in the tests are about 1% lower than the charges used at LASL, and assuming an error of ∿1% in measuring the detonation velocity and shock velocity, an analysis of equations and indicates the detonation pressure of 179 kbar may be ∿4% too low. This measured value of the detonation pressure is ∿10% lower than the pressure of 201 kbar which was estimated at LASL from work with larger charges.

V. CONCLUSIONS

1. Amatex-20, with either 500 micron or 10 micron particle size AN, can be initiated satisfactorily with a standard A-5 booster.

2. No differences in the initiation of the A-5 booster are found when detonator base charge weights of 40 and 80 mg of PETN, respectively, are used.

3. The measured detonation velocity of Amatex-20 charges containing 500 micron AN was 6790 ± 20 m/sec. Detonation velocities inferred from wave profile measurements, in the wave arrival experiment, were slightly greater for the charges containing 10 micron AN than for those containing 500 micron AN.

4. The measured detonation pressure of Amatex-20 containing 500 micron AN was 179 kbar, for a cast charge with a density of 1.60 g/cc. This value, obtained in the aquarium experiment, is about 10% smaller than that reported by LASL, where larger charges were used.

(18) University of California, Los Alamos Scientific Laboratory, Los Alamos, New Mexico, "Feasibility of Using Amatex in Small Bombs, Progress Report June 16 through August 30, 1974", AFTL Project Order 4, 065Q-111.

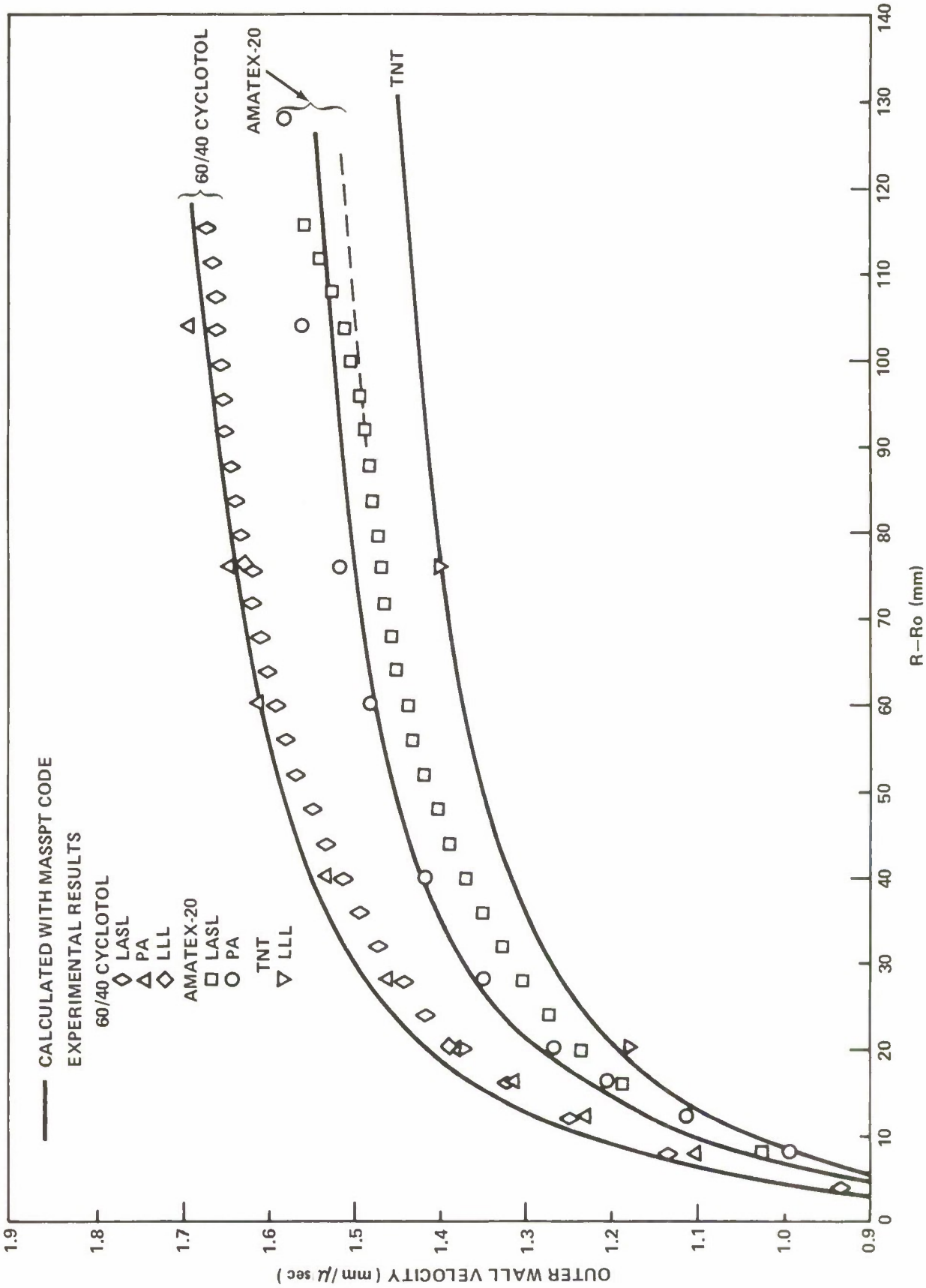

FIG. 1 CALCULATED AND EXPERIMENTAL OUTER WALL VELOCITIES OBTAINED WITH LLL CYLINDER TEST SCALED UP TO 4 INCH INSIDE DIAMETER. RESULTS FOR 60/40 CYCLOTOL, AMATEX-20, AND TNT ARE COMPARED.

BLU–61B

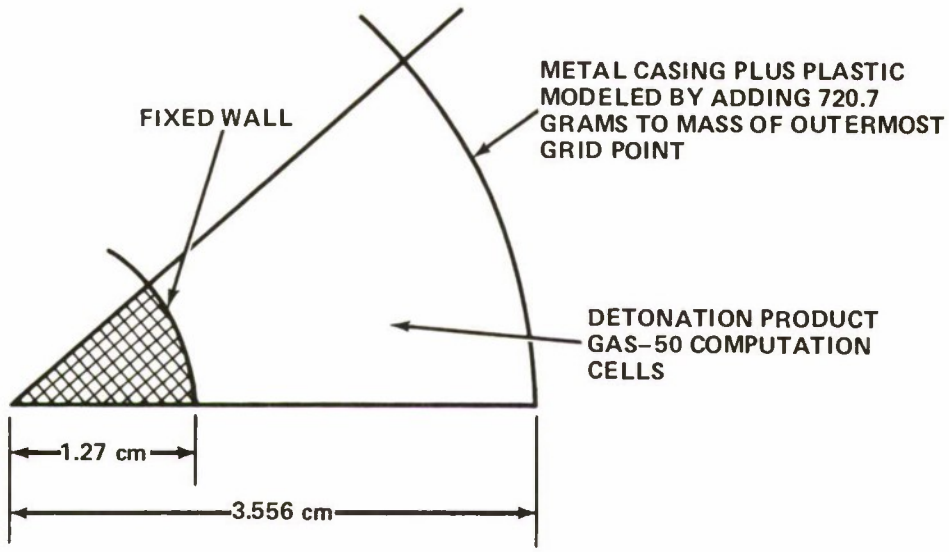

BLU–63B

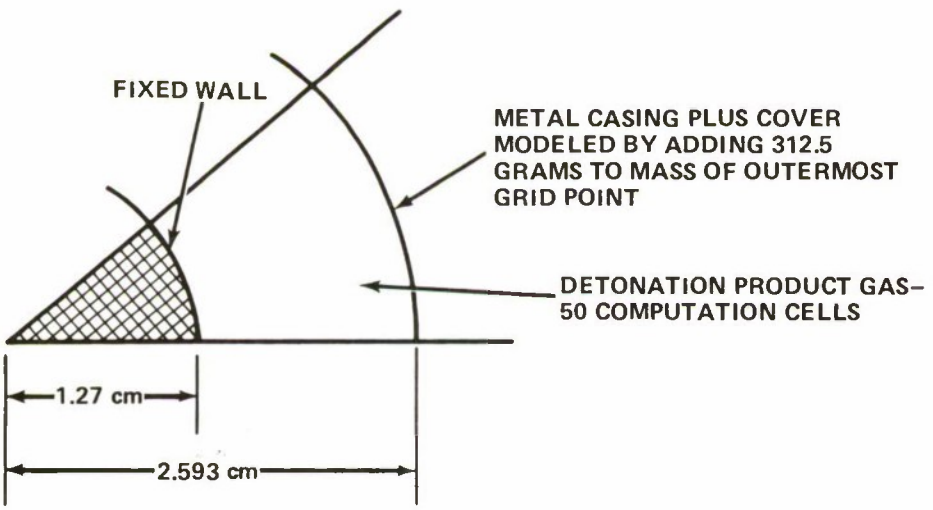

FIG. 2 DIMENSIONS USED FOR SPHERICAL FLOW COMPUTATIONS.

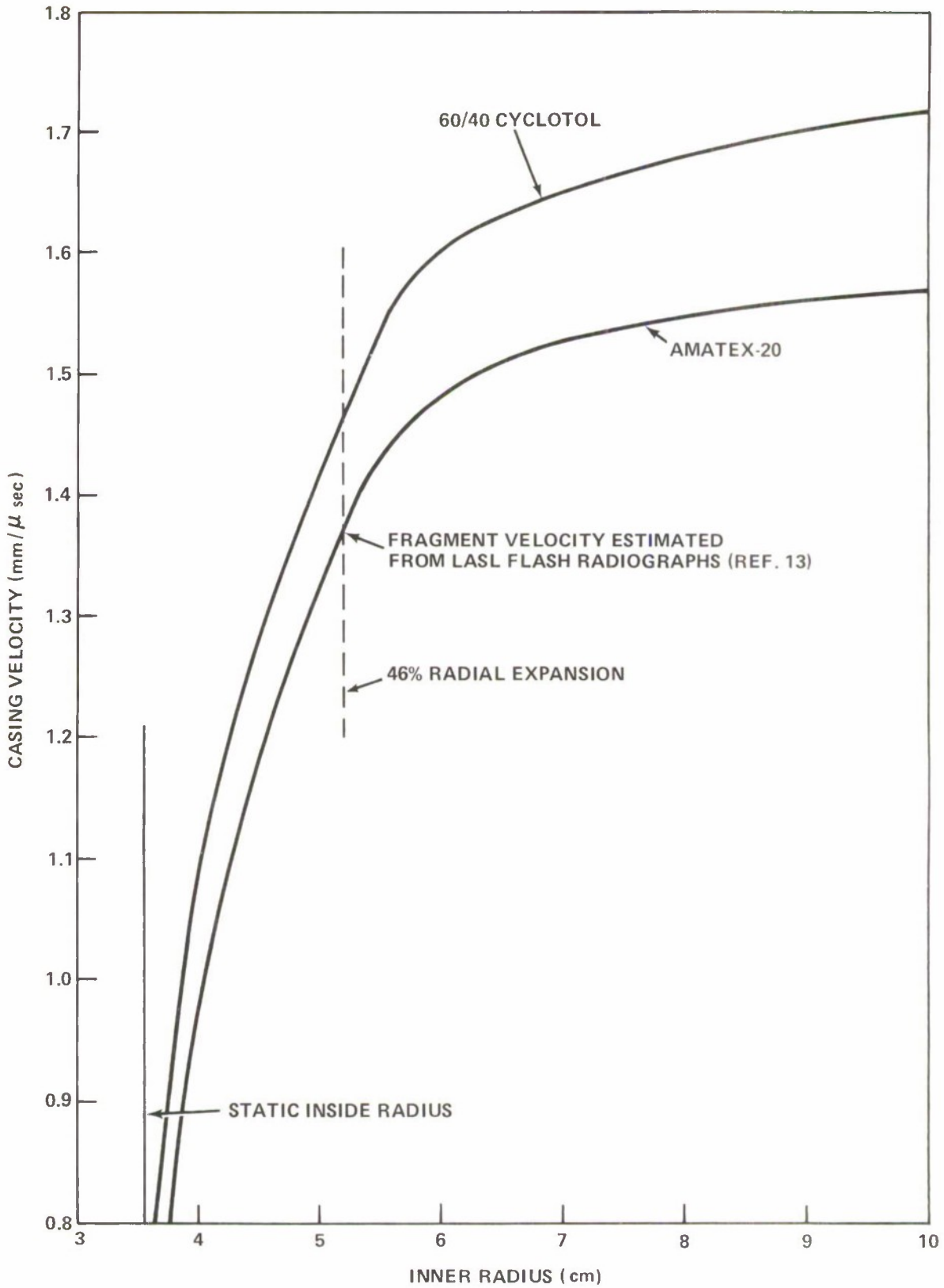

FIG. 3 BLU-61B SUBMUNITION. CALCULATED CASING VELOCITY AT 70° POSITION VS INSIDE RADIUS, FOR 60/40 CYCLOTOL AND AMATEX-20 FILLS.

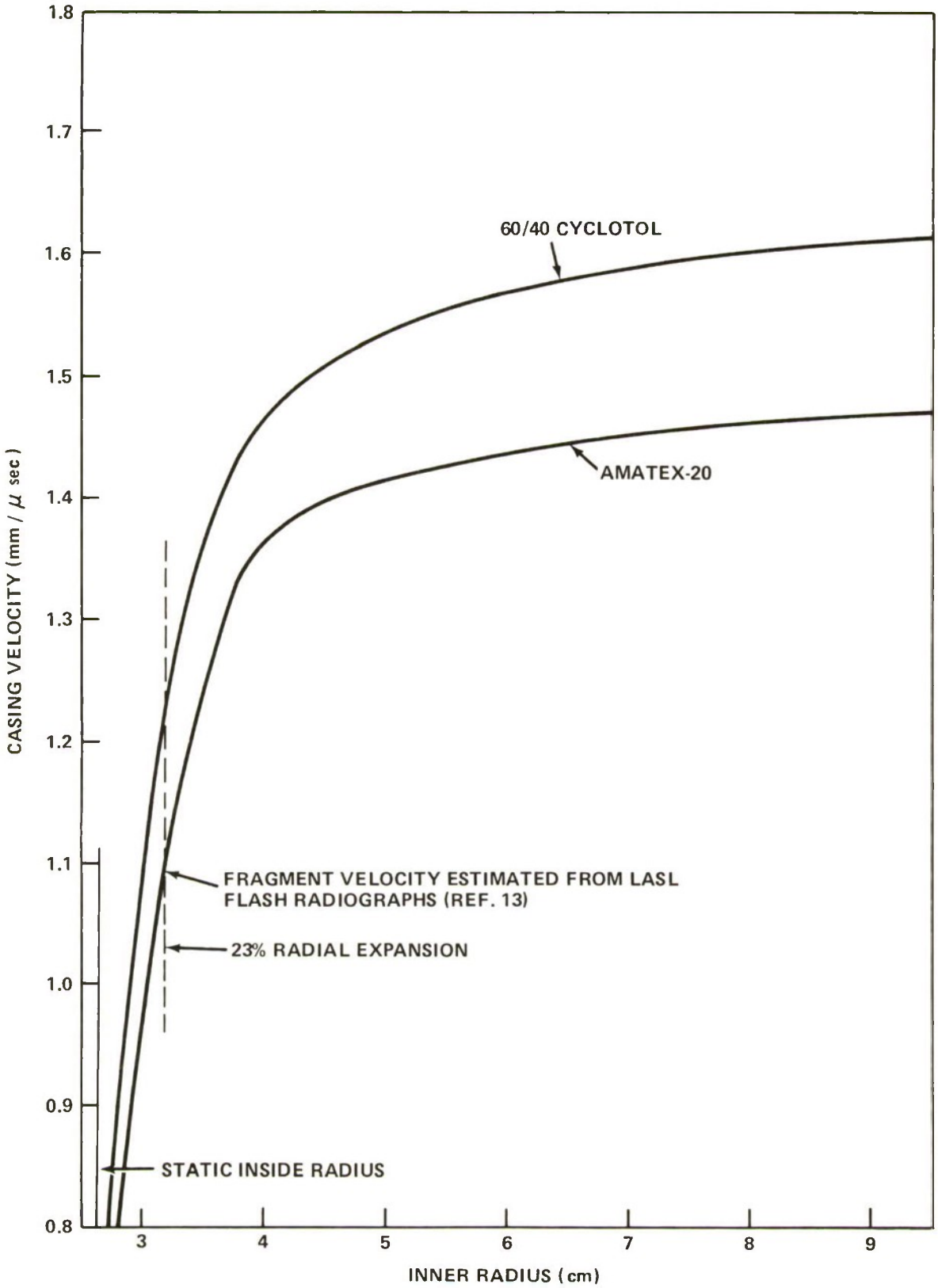

FIG. 4 BLU - 63B SUBMUNITION. CALCULATED CASING VELOCITY AT 70° POSITION VS INSIDE RADIUS, FOR 60/40 CYCLOTOL AND AMATEX-20 FILLS.

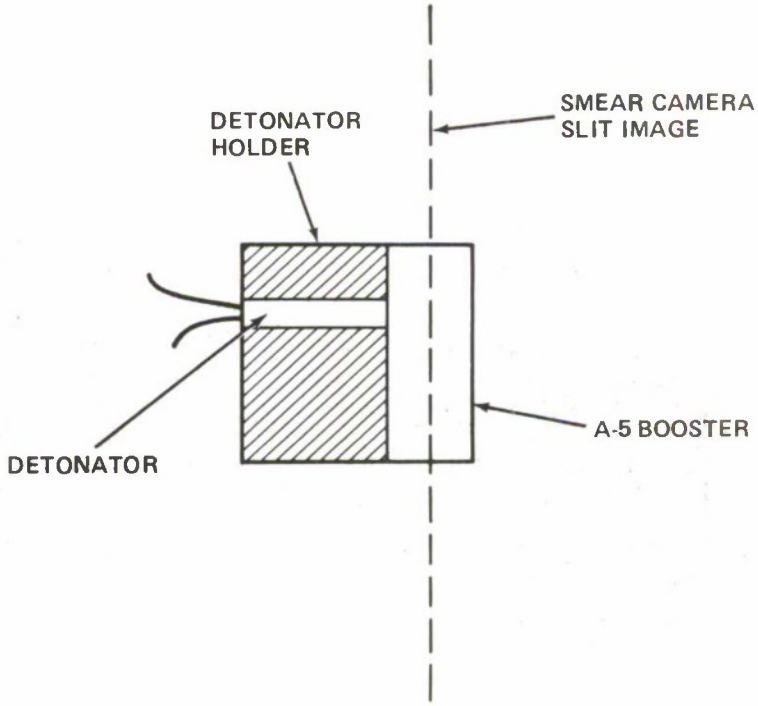

FIG. 5A ARRANGEMENT FOR LATERAL SHOCK OUTPUT MEASUREMENTS FROM A-5 BOOSTERS VS DETONATOR BASE CHARGE WEIGHT.

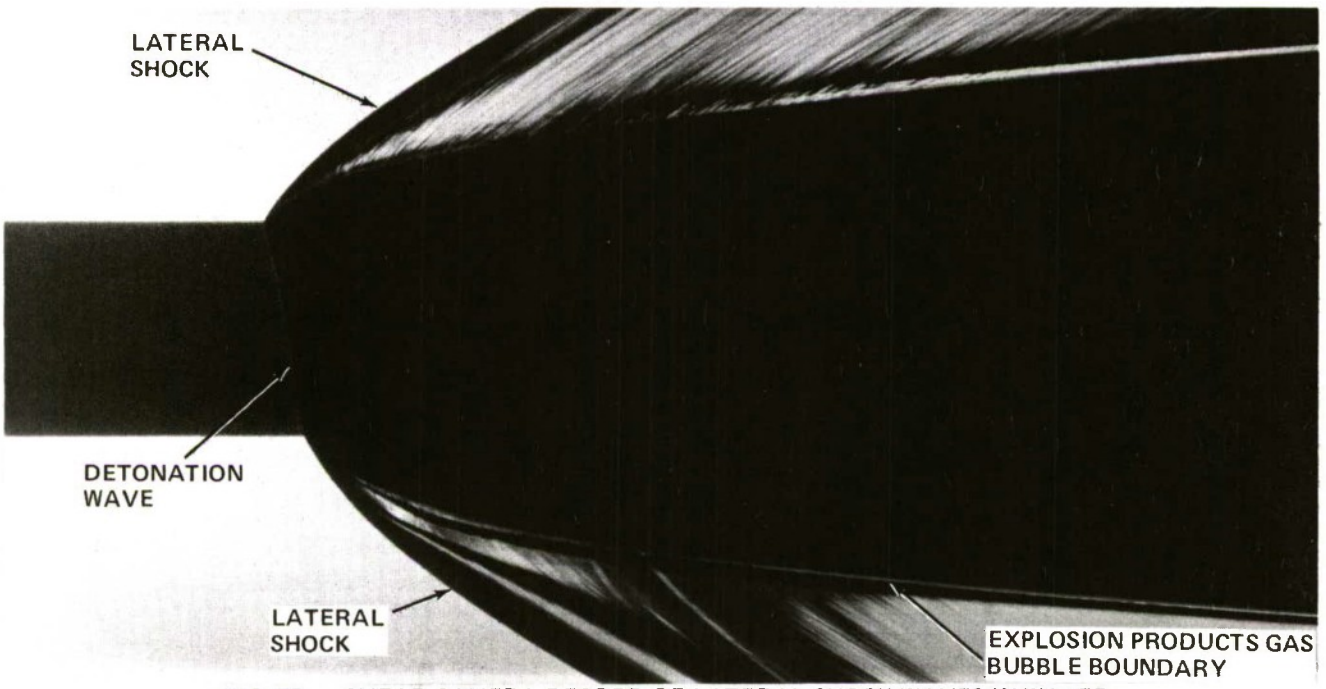

FIG. 5B SMEAR CAMERA RECORD OF LATERAL SHOCK WAVES IN WATER FROM DETONATION OF AN A-5 BOOSTER.

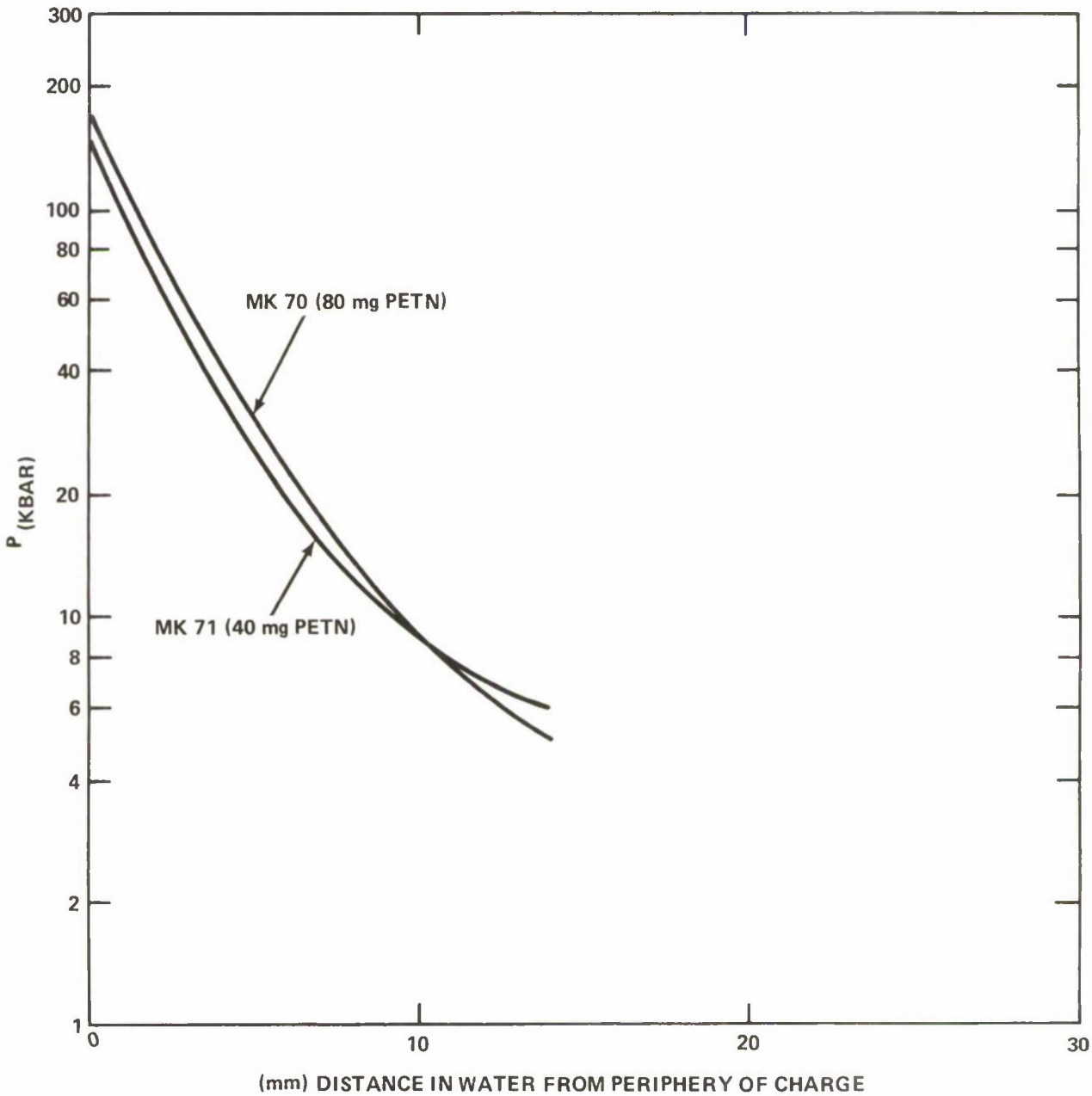

FIG. 6 LATERAL PEAK PRESSURE VS DISTANCE IN WATER FROM THE PERIPHERY OF A-5 BOOSTERS. (WEAK SHOCK)

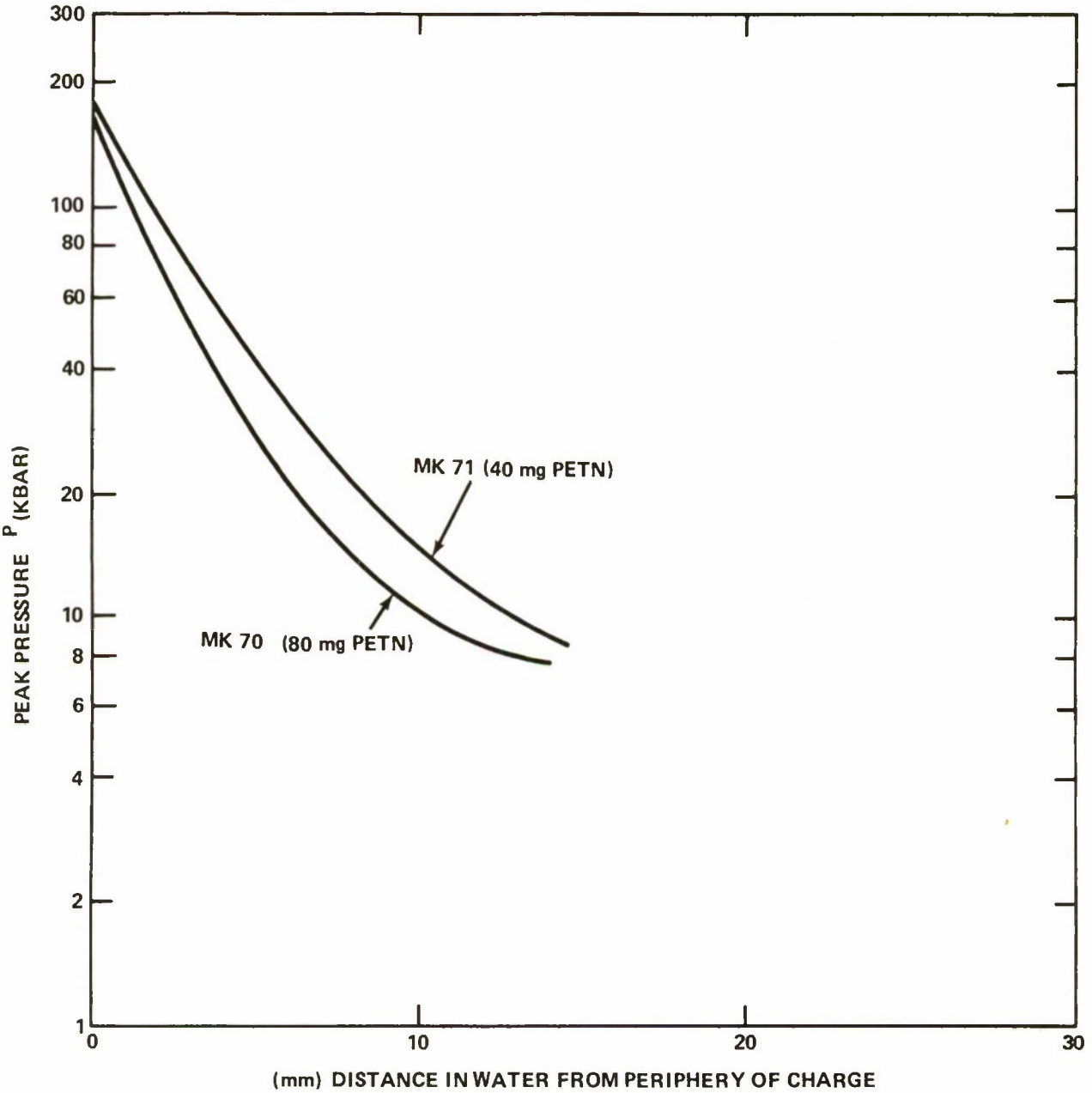

FIG. 7 LATERAL PEAK PRESSURE VS DISTANCE IN WATER FROM THE PERIPHERY OF A-5 BOOSTERS. (STRONG SHOCK)

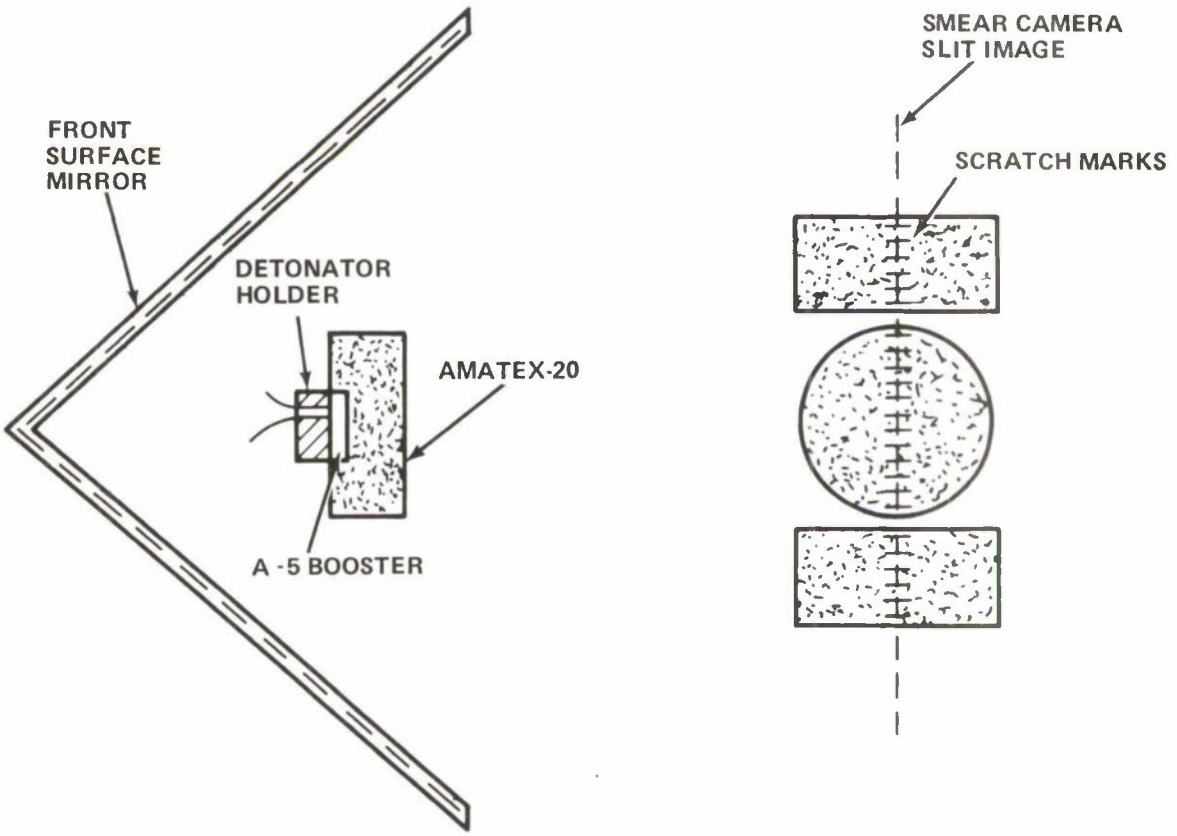

FIG. 8 ARRANGEMENT FOR DETONATION WAVE ARRIVAL MEASUREMENTS ON THE PERIPHERY AND FACE OF AMATEX-20 CYLINDER CHARGE

FIG. 9 SMEAR CAMERA RECORD OF DETONATION WAVE ARRIVAL ON THE PERIPHERY AND FACE OF A CYLINDRICAL AMATEX-20 CHARGE

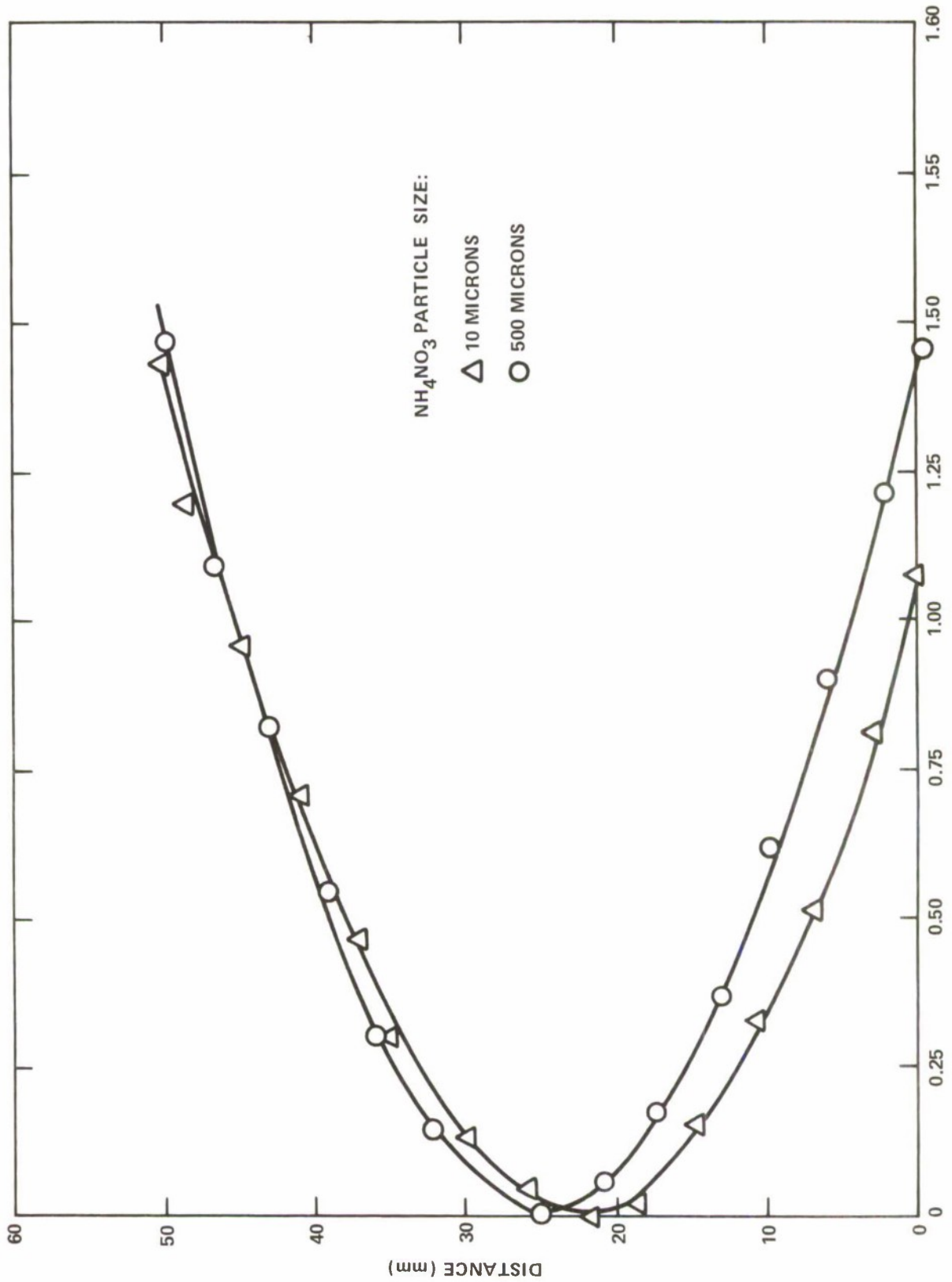

FIG. 10 DETONATION WAVE ARRIVAL TIME DIFFERENCES AT POINTS ON THE FACE OF AN AMATEX-20 CYLINDER INITIATION: MK 71 DETONATOR, A-5 BOOSTER.

DISTRIBUTION

COMMANDER
NAVAL SEA SYSTEMS COMMAND
DEPARTMENT OF THE NAVY
WASHINGTON, D.C. 20362
SEA-09G32 2
SEA-03
SEA-033
SEA-034
SEA-0332

COMMANDER
NAVAL AIR SYSTEMS COMMAND
WASHINGTON, D.C. 20361
AIR-LIBRARY
AIR-035(E.FISHER)

CHIEF OF NAVAL MATERIAL (CNM-PM-1)
WASHINGTON, D. C. 20360
NAVMAT-0323 (I. JAFFE)
SP-43 (LIBRARY)

CHIEF OF NAVAL RESEARCH
ARLINGTON, VIRGINIA 22217
TECHNICAL LIBRARY
ONR-473

DIRECTOR
NAVAL RESEARCH LABORATORY
WASHINGTON,D.C.,20930
TECH. INFORMATION

COMMANDER
NAVAL WEAPONS CENTER
CHINA LAKE, CALIFORNIA 93555
TECHNICAL LIBRARY
H. GRYTING
R. G. SEWELL
R.REED
C.D.LIND

NAVAL ACADEMY
ANNAPOLIS, MARYLAND 21402
HD. WEPS DEPT

COMMANDER
NAVAL SHIP RESEARCH AND DEVELOPMENT CENTER
BETHESDA, MARYLAND 20034
LIBRARY

COMMANDER
NAVAL AIR DEVELOPMENT CENTER
JOHNSVILLE, PENNSYLVANIA 18974
AVIATION ARMAMENT LABORATORIES

SUPERINTENDENT
NAVAL POSTGRADUATE SCHOOL
MONTEREY, CALIFORNIA 93940
LIBRARY

COMMANDER
NAVAL WEAPONS STATION
YORKTOWN, VA, 23491
RESEARCH AND DEVELOPMENT DIVISION
W. MCBRIDE

COMMANDING OFFICER
NAVAL ORDNANCE STATION
INDIAN HEAD, MARYLAND 20640
LIBRARY
W.F.MCQUISTION

DIRECTOR
ARMY MATERIEL SYSTEMS ANALYSIS AGENCY
ABERDEEN PROVING GROUND
ABERDEEN, MARYLAND 21005
LIBRARY
J.C.C. LIU
M. RECHES
J.SPERAZZA
A.L.YOUNG

COMMANDING GENERAL
ABERDEEN PROVING GROUMD
ABERDEEN, MARYLAND 21005
BALLISTICS RESEARCH LABORATROY
TECHNICAL LIBRARY
R. FREY
A. DEITRICH
D. DUNN
F.W.GRACE
R. R. KARPP
C. N. KINGERY
R. T. MARUYAMA
P.HOWE
G.HAUVER
V.M.BOYLE

COMMANDING OFFICER
PICATINNY ARSENAL
DOVER, N. J. 07806
LIBRARY
J. HERSHKOWITZ
G. RANDERS-PERHSON
R. F. WALKER
T.JANKUNIS
S.Y.EINBINDER

COMMANDING OFFICER
HARRY DIAMOND LABORATORIES
WASHINGTON, D.C. 20438
LIBRARY
K.WARNER

CHIEF OF RESEARCH AND DEVELOPMENT
DEPARTMENT OF THE ARMY
WASHINGTON, D. C. 20315

U. S. ARMY MISSILE COMMAND
REDSTONE ARSENAL
HUNTSVILLE, ALABAMA 35809
ATTN LIBRARY

COMMANDING OFFICER
FRANKFORD ARSENAL
BRIDGE AND TACONY STS.
PHILADELPHIA,PENNSYLVANIA 19137
LIBRARY
J.REETLE SMUFA L-3200

COMMANDER
U.S. ARMY ARMAMENT COMMAND
ROCK ISLAND, ILLINOIS 61201
LIBRARY

DIRECTOR
U. S. ARMY CORPS OF ENGINEERS
WATERWAYS EXPERIMENT STATION
VICKSBURG, MISSISSIPPI 39180
LIBRARY

COMMANDING GENERAL
U. S. ARMY MATERIEL COMMAND
WASHINGTON, D. C. 20316
O.H.BORUM(AMCRD-TC)
J.V.R.KAUFMAN

COMMANDING OFFICER
U.S. ARMY MOBILITY EQUIPMENT RESEARCH AND DEVELOPMENT CENTER
FORT BELVOIR, VIRGINIA 22060
J.W. BOND, JR.

OOAMA
HILL AFB
OGDEN, UTAH 84401
LIBRARY

COMMANDING OFFICER
AIR FORCE ARMANENT LABORATORY
EGLIN, FLORIDA 32542
LIBRARY
J. CHANDLER (ADTC/TSX)
G. CREWS (AFATL/DLRV)
L. ELKINS
W. D. THOMAS (AFATL/DLYW)
E. M. WINTERMOYER (AFATL/DLKB)
G. M. WISE (ADTC/TSGGL)
M.ZIMMER
D.MADDOX(AFATL/DLYW) 4

COMMANDING GENERAL
AIR FORCE SYSTEMS COMMAND
ANDREWS AIR FORCE BASE
CAMP SPRINGS, MARYLAND 20331
LIBRARY
R.W.HARTMEYER

DIRECTOR
ADVANCED RESEARCH PROJECTS AGENCY
WASHINGTON, D. C. 20301
LIBRARY

U. S. BUREAU OF MINES
DIVISION OF EXPLOSIVE TECHNOLOGY
4800 FORBES AVENUE
PITTSBURGH, PENNSYLVANIA 15212
R.W.VAN DOLAH
R.W.WATSON

DEFENSE DOCUMENTATION CENTER 12
CAMERON STATION
ALEXANDRIA, VIRGINIA 22314

DIRECTOR
INSTITUTE FOR DEFENSE ANALYSIS
400 ARMY-NAVY DRIVE
ARLINGTON, VIRGINIA 22202
LIBRARY

DIRECTOR
DEFENSE RESEARCH AND ENGINEERING
WASHINGTON, D. C. 20305
TECHNICAL LIBRARY

DIRECTOR
DEFENSE NUCLEAR AGENCY
WASHINGTON, D. C. 20305
TECHNICAL LIBRARY

DIRECTOR
JOHN HOPKINS UNIVERSITY
APPLIED PHYSICS LABORATORY
SILVER SPRING, MARYLAND 20910
LIBRARY

IIT RESEARCH INSTITUTE
60 WEST 35TH STREET
CHICAGO, ILLINOIS 60616
H. NAPADENSKY
TECHNICAL LIBRARY

LOS ALAMOS SCIENTIFIC LABORATORY
P. O. BOX 1663
LOS ALAMOS, NEW MEXICO 87544
ATTN LASL LIBRARY
R.CRAIG
W.C.DAVIS
W.E.DEAL
W.FICKETT
C.L.MADER
A.POPOLATO
J. RAMSAY

SYSTEMS,SCIENCE AND SOFTWARE
P.O. BOX 1620
LA JOLLA,CALIFORNIA 92037
R.T.SEDGWICK

WASHINGTON STATE UNIVERSITY
DEPARTMENT OF PHYSICS
PULLMAN, WASHINGTON 99163
DR. G. DUVALL

UNIVERSITY OF CALIFORNIA
LAWRENCE LIVERMORE LABORATORY
P. O. BOX 808
LIVERMORE, CALIFORNIA 94550
TECHNICAL INFORMATION DIVISION
M.WILKINS
M.FINGER
E.JAMES
J.W.KURY
E.L.LEE
F.WALKER
H.HORNIG
H.CHEUNG

SANDIA CORPORATION
P. O. BOX 5800
ALBUQUERQUE, NEW MEXICO 87115
TECHNICAL INFORMATION
J. E. KENNEDY
W. B. BENEDICK

SANDIA CORPORATION
P. O. BOX 969
LIVERMORE, CALIFORNIA 94550

AEROJET-GENERAL CORPORATION
11711 SOUTH WOODRUFF AVENUE
DOWNEY, CALIFORNIA 90241
LIBRARY

HERCULES POWDER COMPANY
RESEARCH CENTER
WILMINGTON, DELAWARE 19899
TECHNICAL INFORMATION CENTER

MARTIN MARIETTA CORPORATION
P. O. BOX 5837
ORLANDO, FLORIDA 32805
MP-30 ENGINEERING LIBRARY

THIOKOL CHEMICAL CORPORATION
HUNTSVILLE DIVISION
HUNTSVILLE, ALABAMA 35809
TECHNICAL LIBRARY

SHOCK HYDRODYNAMICS, INC.
15010 VENTURA BOULEVARD
SHERMAN OAKS, CALIFORNIA 91403
DR. L. ZERNOW
DR. H. ANDERSON

STANFORD RESEARCH INSTITUTE
POULTER LABORATORIES
MENLO PARK, CALIFORNIA 94025
LIBRARY
DR. G. ABRAHAMSON
DR. M. COWPERTHWAITE
DR. R. SHAW

THIOKOL CHEMICAL CORPORATION
HUNTER BRISTOL DIVISION
BRISTOL, PENNSYLVANIA 19007

R. STRESAU LABORATORY
STAR ROUTE
SPOONER, WISCONSIN 54801

DUPONT EASTERN DIVISION
GIBBSTOWN, NEW JERSEY 08027
DR. L. COURSEN

FOREIGN SCIENCE AND TECHNOLOGY CENTER
AMXST-CM-AM
WASHINGTON, D.C. 20360
CAPT BERTI

PANTEX PLANT-DEVELOPMENT DIVISION
MASON AND HANGAR
SILAS MASON CO., INC.
P. O. BOX 647
AMARILLO, TEXAS 79105
TECHNICAL LIBRARY
J. K. RIGDON

HONEYWELL INC.
SYSTEMS AND RESEARCH DIVISION
RESEARCH DEPARTMENT
ST. PAUL, MINNESOTA 55413
E. E. FISHER

FMC CORPORATION
DEFENSE TECHNOLOGY LABORATORY
333 BROKAW ROAD
BOX 520
SANTA CLARA, CALIFORNIA 95052
TECHNICAL LIBRARY
D. R. KENNEDY

HUGHES AIRCRAFT CORPORATION
AEROSPACE GROUP
CULVER CITY, CALIFORNIA 90230
I. G. HENRY

NDW-NSWC(W)-5605/1 (Rev. 1-75)

TO AID IN UPDATING THE DISTRIBUTION LIST FOR NAVAL SURFACE WEAPONS CENTER, WHITE OAK LABORATORY TECHNICAL REPORTS PLEASE COMPLETE THE FORM BELOW:

TO ALL HOLDERS OF NSWC/WOL/TR 75-94
by N. L. Coleburn, Code WR-13

DO NOT RETURN THIS FORM IF ALL INFORMATION IS CURRENT

A. FACILITY NAME AND ADDRESS *(OLD) (Show Zip Code)*

NEW ADDRESS *(Show Zip Code)*

B. ATTENTION LINE ADDRESSES:

C.

☐ REMOVE THIS FACILITY FROM THE DISTRIBUTION LIST FOR TECHNICAL REPORTS ON THIS SUBJECT.

D.
NUMBER OF COPIES DESIRED _____

GPO 885-970

DEPARTMENT OF THE NAVY
NAVAL SURFACE WEAPONS CENTER
WHITE OAK, SILVER SPRING, MD. 20910

OFFICIAL BUSINESS
PENALTY FOR PRIVATE USE, $300

POSTAGE AND FEES PAID
DEPARTMENT OF THE NAVY
DOD 316

U.S.MAIL

COMMANDER
NAVAL SURFACE WEAPONS CENTER
WHITE OAK, SILVER SPRING, MARYLAND 20910

ATTENTION: CODE WR-13